J Mater Sci (2007) 42:6614–6627
DOI 10.1007/s10853-007-1512-2

Growth of boride layers on the 13% Cr steel surface in a mixture of amorphous boron and KBF_4

V. I. Dybkov

Received: 18 March 2006 / Accepted: 9 January 2007 / Published online: 2 May 2007

Abstract Two borides FeB and Fe_2B were found to form as separate layers at the interface between a 13% Cr steel and boron at 850–950 °C and reaction times up to 12 h. The average chromium content is 8 at.% in the FeB layer and 9 at.% in the Fe_2B layer. Both layers are characterized by a pronounced texture. The strongest reflections are {002} and {020} for the orthorhombic FeB phase and {002} for the tetragonal Fe_2B phase. Diffusional growth kinetics of boride layers are close to parabolic and can alternatively be described by a system of two non-linear differential equations, producing a good fit to the experimental data. Annealing of a borided steel sample in the absence of boriding media results in disappearance of the FeB layer. Microhardness values are 17.9 ± 1.5 GPa for the FeB layer, 16.1 ± 0.9 for the Fe_2B layer and 5.9 ± 0.3 GPa for the steel base. The abrasive wear resistance of the FeB layer is 25 times greater than that of the steel base. The Fe_2B layer yields about a 15-fold increase in wear resistance of steel samples.

Introduction

Boriding is one of the widespread thermochemical surface treatments used to improve mechanical and corrosive wear resistance, hardness and other service characteristics of metals, alloys and steels [1–3]. Iron borides Fe_2B and FeB exist in the Fe–B binary system [4–7]. Therefore, with iron, its alloys and steels, either one-phase or two-phase coatings can be obtained, depending on boriding media employed and temperature-time conditions of a boriding procedure.

Note that even if three or more compounds exist in the metal-boron binary system, in most cases only two of them form separate layers at the interface between reacting phases [8]. This contradicts diffusional considerations [9] predicting the simultaneous formation and subsequent parabolic growth of the layers of all compounds of any binary system, whatever their number, but agrees with a physicochemical viewpoint [10], according to which one or two layers can occur and grow simultaneously under conditions of diffusion control, with other compound layers being skipped for kinetic reasons.

Boriding at 950 °C for 6 h in a mixture of 30% SiC and 70% $Na_2B_4O_7$ is known to produce a coating of a thickness of 15 μm on the surface of the 30X13 (0.30% C and 13% Cr) steel material [11], similar to that material employed in this investigation. With a mixture of 30–35% B_4C and 70–65% $Na_2B_4O_7$ and the $Na_2B_4O_7$ melt (electrolysis), appropriate thickness values are 40 and 55 μm, respectively. Mixtures of amorphous boron and KBF_4 appear to be more effective boriding agents due to the formation of a gas phase (mainly BF_3) at elevated temperatures [1, 8, 11]. In this work, the results of investigation of the interaction of a commercial 40X13 steel and boron in a mixture of amorphous boron powder and 5% KBF_4 at 850–950 °C are presented, with the main emphasis on establishing the boride layer-growth kinetics that received comparatively little attention. Also, the results of dry abrasive wear resistance tests of boride coatings formed on the steel-material surface are presented.

V. I. Dybkov (✉)
Department of Physical Chemistry of Inorganic Materials,
Institute for Problems of Materials Science,
Kyiv 03180, Ukraine
e-mail: vdybkov@ukr.net
URL: http://users.i.com.ua/~dybkov/V

Experimental procedure

Materials and specimens

The materials used included a 40X13 steel rod (16 mm diameter) in the as-received condition (without any additional heat treatment), amorphous boron and analytical-grade KBF_4. The content of main components of the steel was 85.2% Fe, 13.6% Cr, 0.38% C, 0.30% Mn, 0.30% Si and 0.20% Ni. All contents are given in mass percent if otherwise not stated. The steel microstructure consisting of the body centered cubic α-phase (ferrite) and carbides $Me_{23}C_6$ (Me = Cr, Fe) is shown in Fig. 1.

Initially, the boron powder contained 98.3% B, 0.04% C, 1.6% O and insignificant amounts of Si, Cu, Mg (< 0.01% each) and Fe (< 0.001%). Before the boriding experiments, the powder was first heated slowly in vacuum up to 1,450 °C and then calcined at this temperature for 2 h in an atmosphere of argon at a pressure of 2.5×10^4 Pa to remove volatile oxides. Subsequently, it was cooled by filling the chamber with argon at atmospheric pressure. The average cooling rate (to 200–250 °C) was around 2 °C s^{-1}. After this treatment, no significant changes of the powder morphology and structure were revealed, except for the beginning of resolution of some broad X-ray diffraction peaks. KBF_4 was preliminary dried in steps at 95, 110, 130 and 170 °C (24 h at each temperature).

Specimens in the form of tablets, 11.28 mm diameter and 5.5 mm high, were machined from the steel rod. Flat sides (1 cm^2 area) of the tablets were ground and polished mechanically.

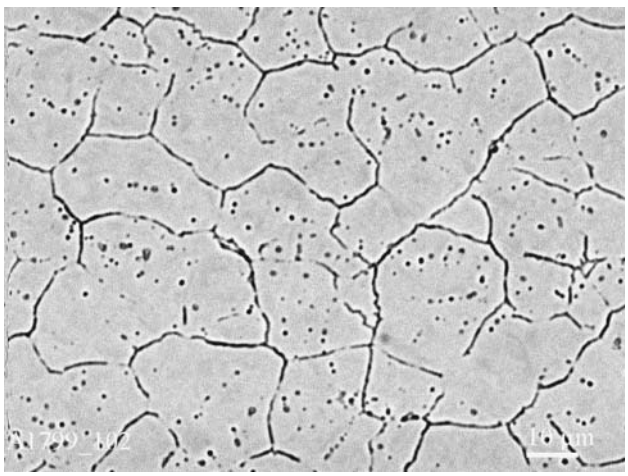

Fig. 1 The 13% Cr steel microstructure. Polished mechanically and etched for 60 s in a solution of 4 ml HF and 8ml HNO_3 in 100 ml ethanol at room temperature

Experimental methods

The vacuum device VPBD-2S employed for boriding steel samples has been described elsewhere [12]. The experiment was carried out in an alumina crucible, 13 mm inner diameter and 40 mm high.

A steel tablet was embedded into a mixture of boron powder with 5% KBF_4 as an activator. This amount of KBF_4 appears to be optimum [1, 8]. The mixture was then slightly pressed, and a load of 8.5 g (a low-carbon steel cylinder) was placed on top. The crucible was closed with a low-carbon steel lid and placed into a steel-sheet holder, mounted to a guide rod capable of moving in the vertical direction.

The chamber was pumped to a pressure of about 10 Pa and filled with high-purity argon (99.999 vol.% Ar). This procedure was repeated twice. Then, the chamber was again pumped and filled with argon at a pressure of 2.5×10^4 Pa, and heating was started. During heating, the crucible with its contents was in the cold zone above the furnace. After the required temperature in the range of 850–950 °C had been reached in the furnace, the crucible, pre-heated to about 400 °C, was moved into its middle part. After an initial drop, the temperature attained its predetermined value in 4–5 min and was then maintained constant within ± 1 °C with the help of an automatic thermoregulator VRT-3. The temperature measurements were carried out using a Pt–PtRh thermocouple. The experiments were performed at temperatures of 850, 900 and 950 °C. Their duration was 3,600–43,200 s (1–12 h).

After the experiment, the steel tablet coated with boride layers was cut along the cylindrical axis into two unequal parts (4 and 7 mm) using an electric-spark machine. The greater part of the tablet was embedded into a cold-setting epoxy resin and used to prepare a metallographic cross-section. The lesser part was used for X-ray diffraction investigations (plain-view samples).

Characterization of the steel and boride layers was carried out with the help of metallography, X-ray (XA) and chemical (CA) analyses, and electron probe microanalysis (EPMA). The thickness of boride layers was measured using an optical microscope MIM-7 equipped with a HP Photosmart 720 camera. Eight to ten measurements were made at different places of the interface (~1 cm long on any cross-section) between the reacting phases and the average value of the layer thickness was found. The mean relative error of its determination was around ±12%.

The chemical composition of the layers and the concentration profiles of the elements in the steel-boron transition zone were obtained using electron probe microanalyzers JEOL Superprobe 733 and CAMECA

Camebax SX50. The beam spot diameter and the phase volume analyzed at each point were estimated to be about 1 and 2 μm^3, respectively.

X-ray diffraction patterns were taken immediately from the surface of tablet samples on a DRON-3 apparatus using Cu K_α radiation. When taking the first pattern, no polishing of a borided steel sample was applied (section 0). Then, about 40 μm of a boride layer was removed by grinding and subsequent polishing, and another X-ray diffraction pattern was taken (section I). This procedure was repeated at a step of 20–30 μm until the steel base was reached (sections II-V). Six X-ray diffraction patterns were thus taken on each borided steel sample.

Microhardness measurements on metallographic cross-sections were carried out using a PMT-3 tester with the diamond pyramide (Vickers indenter). The load was 0.98 N (100 g).

Abrasive wear resistance tests were carried out on P180 SiC emery paper tape (main fraction grain size 63 μm, maximum 90 μm) using an AWRD-5 device. The velocity of continuous movement of the tape (30 m long) was 0.35 m s^{-1}, while the gauge length during each test was 27.0 m. The load was 50 N (5.1 kg). The working area of Tablet samples was 1 cm^2.

The wear resistance was determined by means of weighing the samples and measuring their height. The accuracy of weighting measurements (analytical balance) was $\pm 5 \times 10^{-5}$ g. The sample height was measured using a micrometer (±0.005 mm). Layer-by-layer measurements on the same borided sample allowed the wear characteristics of different boride phases as well as the steel base to be determined separately.

Results and discussion

Phase identity and chemical composition of boride layers

Two boride phases were found to form as separate layers at the steel-boron interface at 850–950 °C and reaction times up to 12 h (Fig. 2). Layer-by-layer X-ray analysis (Fig. 3) and a further comparison of our and literature [13] data showed the outer layer bordering the boriding agent to be the FeB phase (Fig. 4 and Table 1), while the inner layer adjacent to the steel base to be the Fe_2B phase (Fig. 5 and Table 2).

As seen from cross-sectional micrographs in Figs. 2 and 3, both layers consist of columnar crystals oriented preferentially in the direction of diffusion. Their characteristic feature is a pronounced texture. The strongest reflections are {002} ($2\theta = 63.2°$ and spacing, $d = 0.148$ nm) and, to a lesser extent, {020} ($2\theta = 32.7°$ and $d = 0.275$ nm) for the orthorhombic FeB phase, and {002} ($2\theta = 42.7°$ and $d = 0.212$ nm) for the tetragonal Fe_2B phase. The change in intensities of those reflections with increasing distance

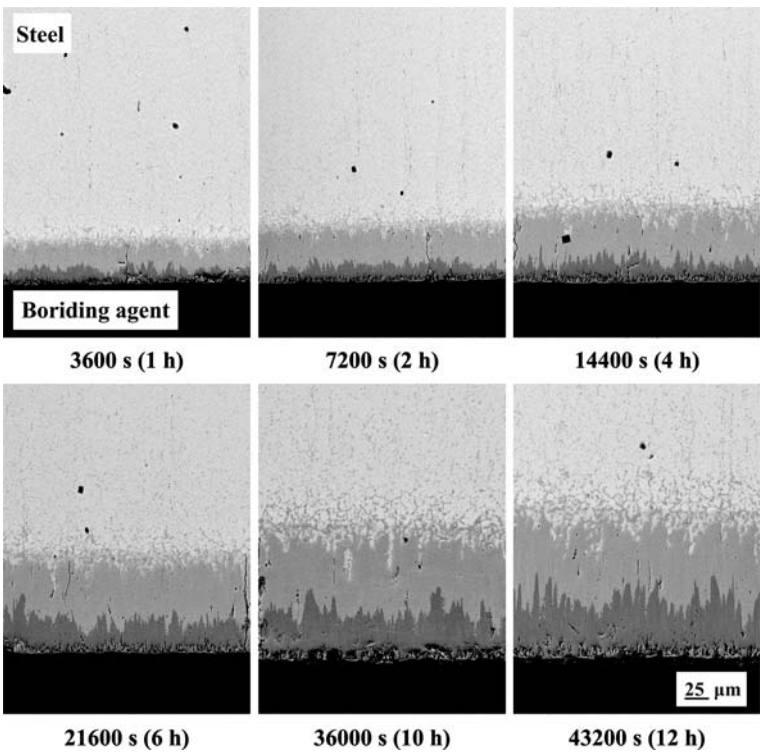

Fig. 2 Backscattered electron images of boride layers formed at the steel-boron interface at a temperature of 950 °C. The darker layer bordering the boriding agent is the FeB phase, while the brighter layer adjacent to the steel base is the Fe_2B phase

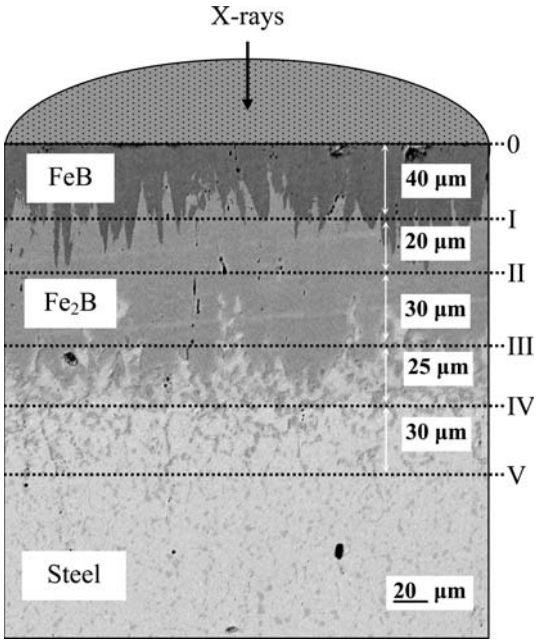

Fig. 3 Scheme of X-ray diffraction experiments

from the surface of a borided steel tablet is illustrated in Table 3. Note that with isotropic microcrystalline samples the strongest reflections are {111}, {200} and {210} for FeB and {211} for Fe_2B.

As seen from Table 3, the larger orientation order is characteristic of the inner portions of both boride layers compared to their near-interface portions, in agreement with findings of other researchers [1, 14, 15]. This is easily explainable because near-interface portions of any boride layer are less equilibrated compared to its inner portions. Therefore, near-interface crystals have less time to align in the preferred direction. The process of formation of the boride-layer texture has been discussed in detail, for example, by Voroshnin and Lyakhovich [1] and recently by Martini et al. [15].

X-ray investigations were followed by EPMA measurements (Table 4). Sections 0 of a borided steel sample corresponded to the FeB phase. Section I crossed both the FeB and Fe_2B phases (Fig. 6 and Table 4). Section II crossed the Fe_2B phase (Fig. 7 and Table 4). Section III was the Fe_2B phase and the steel base in approximately equal amounts. The microstructure of section IV consisted of the steel base with fine inclusions of the Fe_2B phase and an Fe–Cr phase containing 33–53 at.% chromium (Fig. 8 and Table 4). Section V was entirely the steel base of nominal composition.

The FeB and Fe_2B phases dissolve considerable amounts of chromium (Tables 4 and 5). Its distribution within the boride layers is rather irregular (Fig. 9), due probably to non-equilibrium conditions of layer formation. The average chromium content is 8 at.% in the (Fe,Cr)B layer and 9 at.% in the $(Fe,Cr)_2B$ layer. These values agree fairly well with literature ones [14].

Microhardness of boride phases

Microhardness, HV, of the outer (Fe,Cr)B layer was found to be 17.9 ± 1.5 GPa, while that of the inner $(Fe,Cr)_2B$ layer 16.1 ± 0.9 GPa. For the steel base, its value is 5.9 ± 0.3 GPa.

A plot of microhardness values against distance across reacting phases is shown in Fig.10. Microhardness is practically constant within both boride layers and slightly

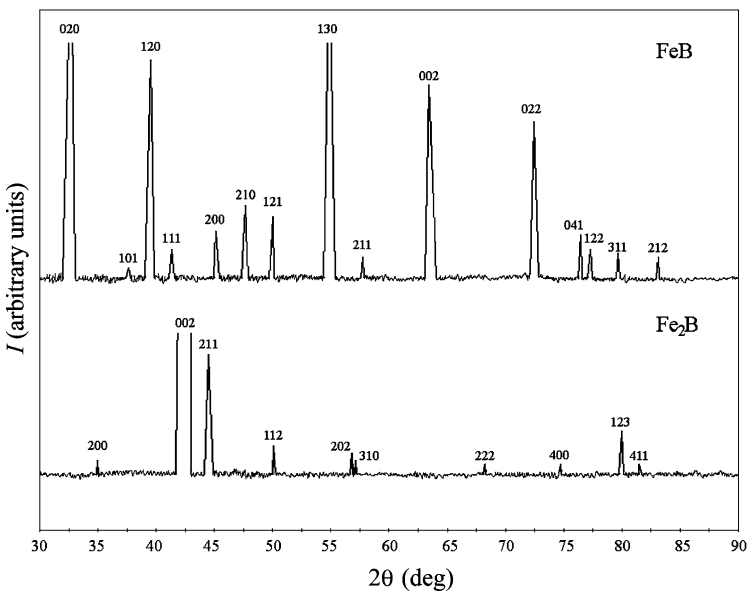

Fig. 4 X-ray diffraction patterns of the FeB (section 0, see Fig. 3) and Fe_2B (section II) phases formed at the steel-boron interface. Boriding conditions: temperature 950 °C, reaction time 21600 s (6 h)

Table 1 Comparison of literature and our experimental X-ray data (*d*-spacing and peak intensities) for the FeB phase (section 0, see Fig. 3) formed at the steel-boron interface at 950 °C and a reaction time of 21600 s (6 h)

Literature data [13]			Our experimental data		
HKL	*d* (nm)	I*	2θ(deg)	*d* (nm)	I
110	0.326	m	27.5	0.3244	vw
020	0.275	s	32.7	0.2738	vs
101	0.240	s	37.5	0.2398	vw
120	0.228	s	39.7	0.2271	s
111	0.219	vs	41.3	0.2181	w
200; 021	0.201	vs	45.2	0.2006	m
210	0.190	vs	47.8	0.1903	s
121	0.181	s	50.0	0.1818	s
130	0.167	s	55.1	0.1667	vs
211	0.160	s	57.5	0.1603	w
002	0.148	m	63.2	0.1471	vs
022	0.1303	m	72.7	0.1301	s
041	0.1249	m	76.6	0.1244	m
122	01239	vs	77.3	0.1234	w
311	0.1199	m	80.6	0.1192	w
212	0.1166	vs	83.1	0.1162	w

*Intensity; vw—very weak; w—weak; m—medium; s—strong; vs—very strong

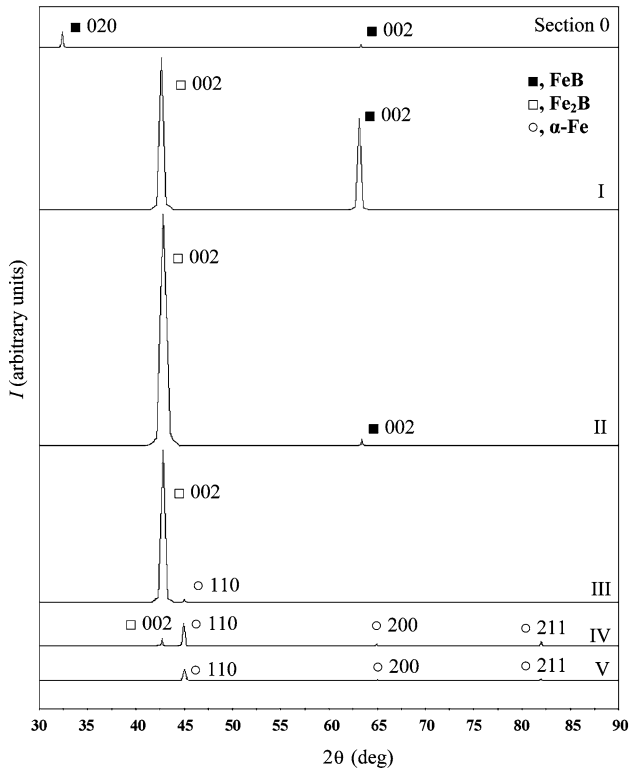

Fig. 5 Most intensive peaks of X-ray diffraction patterns taken from different plain-view sections of a steel sample borided at 950 °C for 21600 s (6 h) (see also Fig. 3 and Table 3)

diminishes (by about 0.2 GPa) in the steel base with increasing distance in the range 0–500μ m from the inner boride layer.

Layer-growth kinetics

Compared to other boriding agents mentioned in Introduction, mixtures of amorphous boron and KBF_4 allow much thicker and more regular boride layers to be obtained under similar conditions of temperature and time. In the presence of BF_3 and other volatile boron-containing compounds, the reaction between steels and boron starts simultaneously over the whole interface. With coarse-grained crystalline boron in the absence of any activator, island-like layers are usually formed, even at a considerable reaction time [1]. In the present case, continuous boride layers arose on the steel surface soon (40–60 s) after the start of the boriding procedure. Note that the gas phase only initiates the reaction, while the further growth of boride layers is a solid-state process.

After compact layers of both borides have formed, their subsequent diffusional growth is due to two partial chemical reactions (Fig. 11)

$$B_{dif} + Fe_2B = 2FeB \quad (1.1)$$

and

$$Fe_{dif} + FeB = Fe_2B. \quad (1.2)$$

Table 2 Comparison of literature and our experimental X-ray data (d-spacing and peak intensities) for the Fe_2B phase (section II, see Fig. 3) formed at the steel-boron interface at 950 °C and a reaction time of 21600 s (6 h)

Literature data [13]			Our experimental data		
HKL	d (nm)	I*	2θ (deg)	d (nm)	I
200	0.256	vw	35.4	0.2536	vw
002	0.212	w	42.7	0.2117	vs
211	0.201	vs	44.8	0.2022	s
112	0.183	m	49.6	0.1838	w
202	0.163	m	56.4	0.1631	w
310	0.161	m	57.6	0.1600	vw
222	0.1371	w	68.0	0.1379	vw
400	0.1277	m	73.7	0.1285	vw
123	0.1202	s	80.0	0.1199	w
411	0.1187	m	81.0	0.1187	vw

* Intensity; vw—very weak; w—weak; m—medium; s—strong; vs—very strong

The growth kinetics of compound layers are usually treated using parabolic equations of the type $x^2 = 2k_1t$, where x is the layer thickness, k_1 is the layer growth-rate constant and t is time [9, 16, 17]. For sufficiently thick layers, such equations produce a quite satisfactory fit to the experimental data (Fig. 12 and Table 6).

In fact, however, growth kinetics of the FeB and Fe_2B layers at the diffusional stage of their formation are somewhat more complicated and can alternatively be described by a system of two non-linear equations [10, 18–21]

$$\frac{dx}{dt} = \frac{k_B}{x} - \frac{rg}{p}\frac{k_{Fe}}{y} \tag{2.1}$$

$$\frac{dy}{dt} = \frac{k_{Fe}}{y} - \frac{q}{sg}\frac{k_B}{x} \tag{2.2}$$

where x is the FeB layer thickness, y is the Fe_2B layer thickness, k_B is the FeB layer growth-rate constant, k_{Fe} is the Fe_2B layer growth-rate constant, g is the ratio of the molar volumes of the FeB and Fe_2B compounds, $p = q = r = 1$ and $s = 2$ (factors from the chemical formulae of FeB and Fe_2B).

Under conditions of diffusion control, both boride layers thicken at their common interface 2, as shown in Fig. 11. The FeB layer grows at the expense of diffusion of the boron atoms across its bulk and their subsequent reaction with the Fe_2B compound. As a result, its thickness increases during dt by dx_{B2}. The Fe_2B layer grows at the expense of diffusion of the iron atoms across its bulk and their further reaction with the FeB compound. During the same time dt, its thickness increases by dy_{Fe2}. Since the FeB and Fe_2B compounds are consumed in the formation of each other, the thickness of the FeB layer simultaneously decreases by dx_-, while that of the Fe_2B layer by dy_-. The net change of the FeB layer thickness during dt is the difference between dx_{B2} and dx_-, while that of the Fe_2B layer thickness is the difference between dy_{Fe2} and dy_-. Therefore, Eqs. (2.1) and (2.2) contain two terms on their right-hand parts.

Even though both boride layers are often considered to grow at the expense of diffusion of the single component

Table 3 X-ray diffraction data showing preferential directions of growth for the FeB and Fe_2B phases formed at the steel-boron interface at 950 °C and a reaction time of 21600 s (6 h)

Phase	HKL	d(nm)	Peak intensity (arbitrary units)					
			0*	I	II	III	IV	V
FeB	020	0.275	203					
	002	0.148	55	1075	93			
Fe_2B	002	0.212		1780	2700	1730	35	
α-Fe	110	0.201				54	95	136
	200	0.143					13	15
	211	0.117					25	27

* Serial numbers of appropriate sections of a borided Tablet sample by a plane parallel to its flat surface (section 0, I and so on, deeper into the sample bulk, see Fig. 3)

Table 4 Average Fe, Cr and B contents of reacting phases, found by EPMA measurements on X-ray diffraction samples (see also Figs. 3, 6–8)

Section	Region	Content (at.%)			Phase
		Fe	Cr	B	
I	Darker in Fig. 6	42.0	8.1	49.9	(Fe,Cr)B
		41.6	7.5	50.9	
		43.5	8.2	48.3	
		41.3	8.7	50.0	
		42.3	9.3	48.4	
	Brighter in Fig. 6	58.6	9.1	32.3	$(Fe,Cr)_2B$
		56.1	9.7	34.2	
		55.5	10.4	34.1	
		57.1	10.4	32.5	
		55.8	9.3	34.9	
II	Brighter in Fig. 7	53.6	11.9	34.5	$(Fe,Cr)_2B$
		54.9	10.8	33.3	
		55.0	10.9	34.1	
	Darker in Fig. 7	39.1	11.3	49.6	(Fe,Cr)B
		39.4	8.8	51.8	
		40.9	10.5	48.6	
IV	Brighter in Fig. 8	85.6	14.4	0.0	Steel base
		83.3	16.7	0.0	
		86.2	13.8	0.0	
	Darker in Fig. 8	34.9	29.4	35.7	$(Fe,Cr)_2B$
		43.0	27.3	29.7	
		40.3	25.3	34.3	
	Grayish in Fig. 8	61.7	38.3	0.0	Fe–Cr
		66.8	33.2	0.0	
		44.8	55.2	0.0	
V		86.1	13.9	0.0	Steel base
		84.7	15.3	0.0	
		85.7	14.3	0.0	

Boriding conditions: temperature 950 °C, reaction time 21600 s (6 h)

boron across their bulks, it is hardly possible with compact layers having no macrodefects and therefore growing by the volume-diffusion mechanism. During diffusional growth, by definition, diffusion across the layer bulks is the rate-determining step, the interface reactions being very fast. It means that all the boron atoms reaching interface 2 react with Fe_2B to form FeB at that interface. Since under conditions of diffusion control the ability of interface 2 to combine those atoms exceeds their diffusional transport across the FeB layer (slow diffusion followed by fast reaction), none of them can diffuse further to interface 3 and react with Fe to form Fe_2B: $B_{dif} + 2Fe = Fe_2B$.

This reaction can only take place either under conditions of reaction control when the flux of boron atoms from the initial B-containing phase is sufficient for both boride layers to grow (for more detail, see Ref. [10]) or if the FeB layer is non-protective due to the presence of cracks and other macrodefects. Reaction-controlled growth is only typical of thin compound layers (< 1 μm thick). The FeB layer was compact and therefore non-permeable to BF_3 and other gases. Hence, neither of these growth mechanisms could be operative with the borides layers investigated.

From a chemical viewpoint, it must thus be clear that the diffusionally growing FeB layer itself can by no means be a source of boron atoms for the Fe_2B layer to grow. Suppose that two FeB molecules decompose at interface 2 to yield one molecule of Fe_2B and one diffusing boron atom: $2FeB = Fe_2B + B_{dif}$. However, this boron atom will be unable to diffuse from interface 2 to interface 3 because under conditions of diffusion control the Fe_2B surface is undersaturated with boron atoms and therefore it is immediately combined at interface 2 according to the reaction $B_{dif} + Fe_2B = 2FeB$. The net result of those reactions is seen to be zero. On the contrary, under conditions of reaction control the Fe_2B surface bordering the FeB layer is oversaturated with boron atoms and therefore part of them (not combined

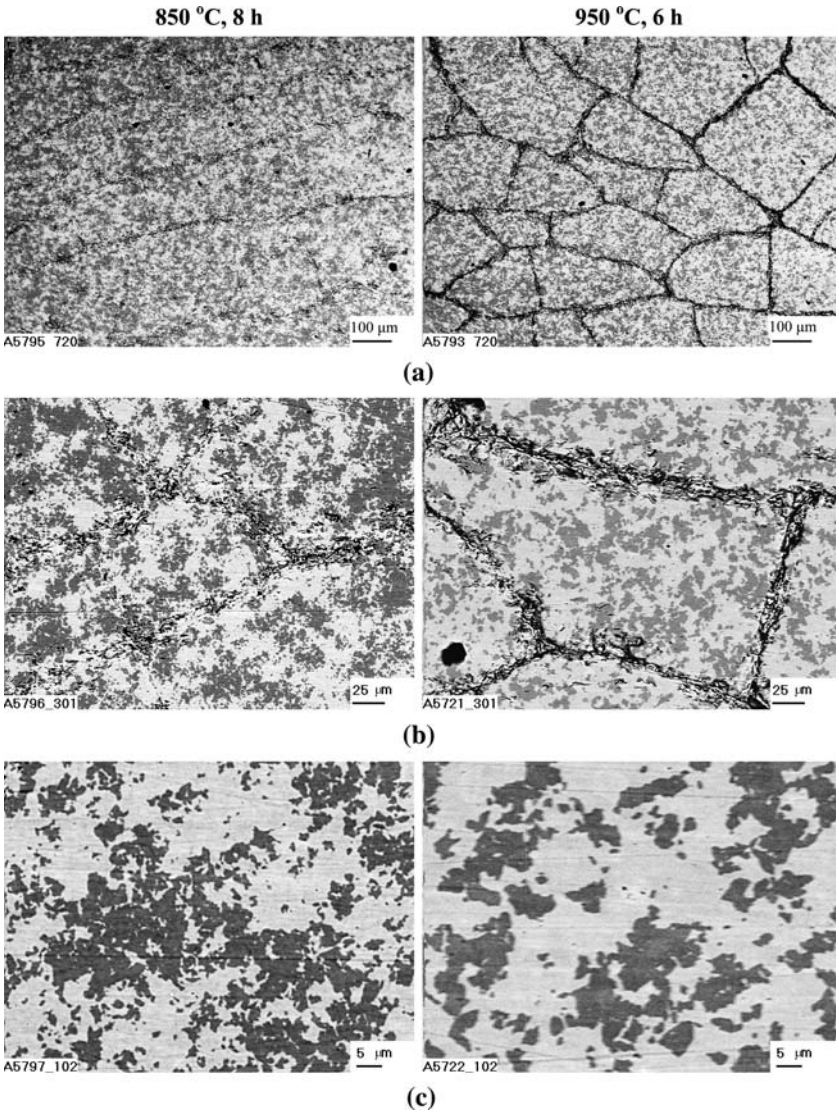

Fig. 6 Plain-view micrographs (backscattered electron images at different magnification) corresponding to section I (see Fig. 3). The darker phase is FeB, while the brighter phase is Fe_2B. Black spots are holes. Penetration of boron along grain boundaries is worth noting

into the FeB phase at interface 2) readily diffuse further to interface 3 and react with iron atoms to form Fe_2B. As the only source of boron atoms for both layers to grow is the boriding mixture (B and KBF_4), it is clear that sooner or later the flux of boron atoms, diminishing as the FeB layer thickens, becomes only sufficient for the FeB layer itself to grow, whereas the faraway Fe_2B layer must stop growing.

Similarly, all the iron atoms diffusing across the Fe_2B layer are combined into Fe_2B by their reaction with FeB at interface 2. Hence, iron atoms cannot take part in the formation of the FeB layer at interface 1. Thus, under conditions of diffusion control both boride (and any other compound) layers only grow at their common interface by pushing each other in opposite directions.

This conclusion is usually overlooked, if the process of formation of compound layers is treated without writing the equations of chemical reactions proceeding at the layer interfaces. In fact, at the diffusional stage of layer formation each of two compound layers without defects can grow only at the expense of diffusion of the atoms of a neighboring initial phase.

Even though grain-boundary diffusion might also contribute to the layer-growth process, its contribution appears to be much less compared to that of volume diffusion in view of the coarse-grained structure of both layers. Therefore, in spite of the considerable difference in values of grain-boundary diffusion and volume diffusion coefficients, the flux of diffusing atoms along grain boundaries could hardly be large.

An obvious criterion of the applicability of Eqs. (2) for treating the diffusional layer-growth kinetics is the constancy of k_B and k_{Fe} over a given range of time, as is the case with boride layers (Table 6). The value of g necessary for calculations of k_B and k_{Fe} was estimated from the densities, $\rho_1 = 6.70 \times 10^3$ kg m^{-3} and $\rho_2 = 7.34 \times 10^3$ kg m^{-3}, of the FeB and Fe_2B compounds [1] and their

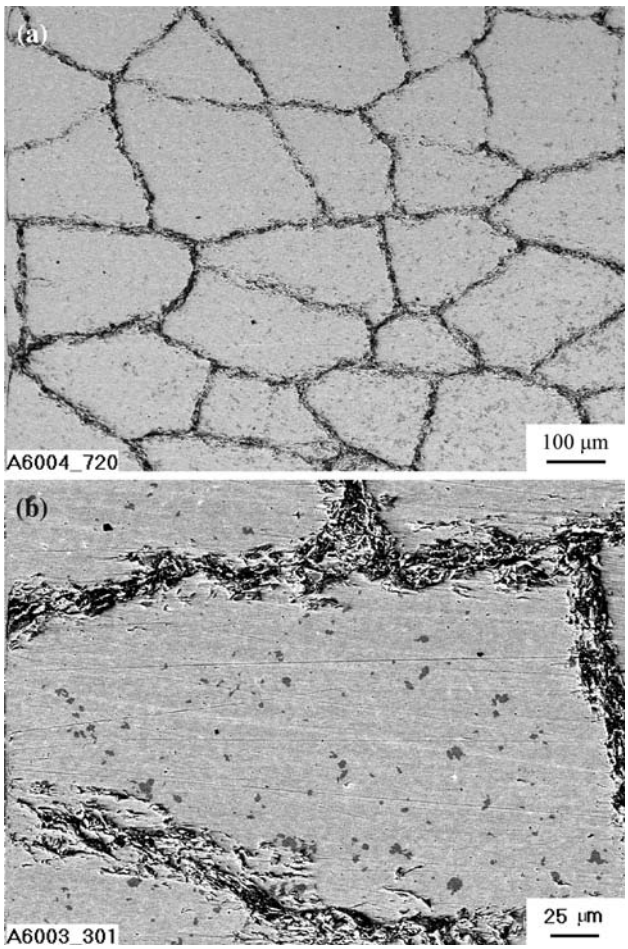

Fig. 7 Plain-view micrographs (backscattered electron images at different magnification) corresponding to section II (see Fig. 3). The main phase is Fe_2B (bright). Inclusions of FeB (darker) are fine and rare. Penetration of boron along grain boundaries is worth noting

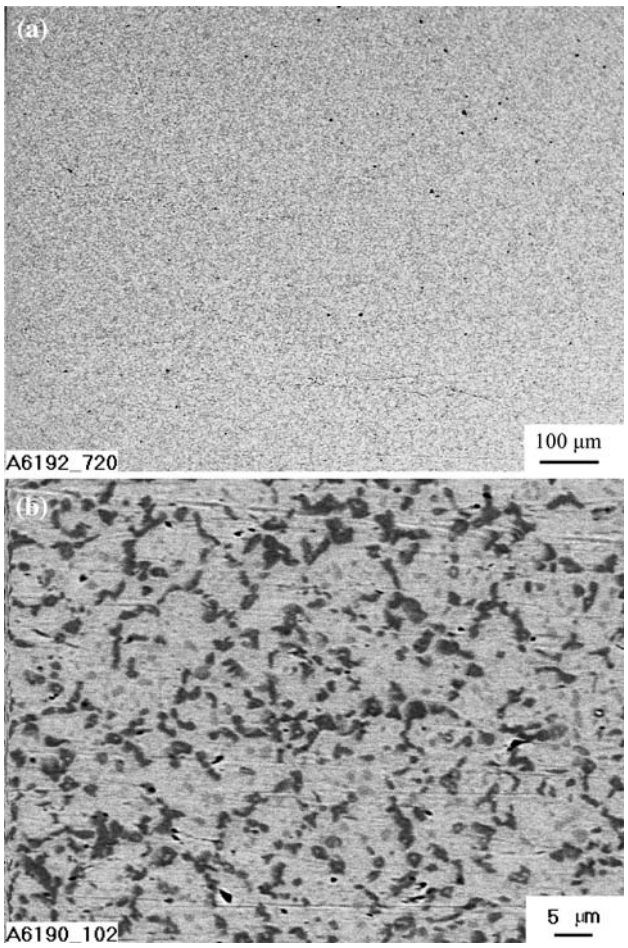

Fig. 8 Plain-view micrographs (backscattered electron images at different magnification) corresponding to section IV (see Fig. 3). The brighter phase is the steel base, while the darker phase is Fe_2B. The steel base is non-homogeneous. Its grayish regions are enriched in chromium

molecular masses, $M_1 = 66.65$ g mol^{-1} and $M_2 = 122.49$ g mol^{-1}: $g = M_1 \rho_2/M_2\rho_1 = 0.60$.

The derivatives were found from the experimental layer thickness-time dependences by the numerical three-point method using a conventional computer program (linear approximation). To find a derivative for a given experimental point, (x_i, t_i), like those on left-hand plots of Fig. 12, data for two neighboring points, (x_{i-1}, t_{i-1}) and (x_{i+1}, t_{i+1}), were also used. Left-hand and right-hand derivatives, $(x_i - x_{i-1})/(t_i - t_{i-1})$ and $(x_{i+1} - x_i)/(t_{i+1} - t_i)$, were first found for this point and a mean value was then calculated. The derivatives could thus be found for all experimental points, excepting clearly end ones, for which a neighboring point is lacking.

As seen in Table 6, the results of calculations of k_B and k_{Fe} are strongly dependent upon a scatter of experimental points. To avoid this, approximation of experimental data with any suitable analytical function is therefore advisable. For example, the use of parabolic relations to approximate the layer thickness-time dependences and then to find the derivatives yields another set of values of k_B and k_{Fe} (Table 7). Since the experimental x–t dependences become smoothed as a result of this procedure (solid lines on left-hand plots of Fig. 12), all values of k_B thus found are identical. The same applies to k_{Fe}. Comparing these with the average values of k_B and k_{Fe} found numerically from the experimental points, it may be concluded that both sets of the constants agree fairly well, providing evidence for the validity of the analytical treatment employed.

The temperature dependence of the layer growth-rate constants is described in the 850–950 °C range by the following equations of the Arrhenius type (Fig. 13)

$$K = K_0 \exp(-E/RT) \tag{3}$$

where K stands for any layer growth-rate constant, E is the activation energy, R is the gas constant and T is the absolute temperature (Fig. 10):

Table 5 EPMA data for the steel-boron diffusion zone. Temperature 950 °C, reaction time 21600 s (6 h)

Phase	Place of measurement	Content (at.%)			Remarks
		Fe	Cr	B	
	At distance l away from the steel-boride layer interface				
Steel	l = –150 μm	86.8	13.2	0.0	< Fe >
	–80	78.5	17.8	3.7	
	–50	87.0	13.0	0.0	
	–20	89.8	10.1	0.0	
	–10	82.7	10.7	6.6	
Inner boride layer	10	56.5	9.2	34.3	$(Fe,Cr)_2B$
	20	59.2	9.0	31.8	
	30	54.8	10.7	34.6	
	40	60.9	9.2	30.0	
	50	61.7	6.4	31.9	
Outer boride layer	60	40.9	7.4	51.7	(Fe,Cr)B
	70	43.3	8.6	48.1	
	80	42.1	7.2	50.7	
	90	43.3	8.5	48.2	

$$k_1 = 1.46 \times 10^{-7}\exp(-149.4\,\mathrm{kJ\,mol^{-1}}/RT)\,\mathrm{m^2\,s^{-1}}$$

for the FeB layer,

$$k_1 = 7.87 \times 10^{-9}\exp(-116.4\,\mathrm{kJ\,mol^{-1}}/RT)\,\mathrm{m^2\,s^{-1}}$$

for the Fe_2B layer,

$$k_1 = 1.36 \times 10^{-7}\exp(-132.8\,\mathrm{kJ\,mol^{-1}}/RT)\,\mathrm{m^2\,s^{-1}}$$

for both boride layers,

$$k_B = 4.40 \times 10^{-7}\exp(-142.2\,\mathrm{kJ\,mol^{-1}}/RT)\,\mathrm{m^2\,s^{-1}},$$

$$k_{Fe} = 1.24 \times 10^{-7}\exp(-124.3\,\mathrm{kJ\,mol^{-1}}/RT)\,\mathrm{m^2\,s^{-1}}.$$

Degradation of boride layers during annealing in the absence of boriding media

Annealing of a borided steel sample (Fig. 14a) in vacuum in the absence of the boriding mixture (B and KBF_4) results in a decrease of the thickness of the FeB layer and an appropriate increase of the thickness of the Fe_2B layer due to the reactions

$$2FeB = Fe_2B + B_{dif} \quad (4)$$

and

$$B_{dif} + 2Fe = Fe_2B \quad (5)$$

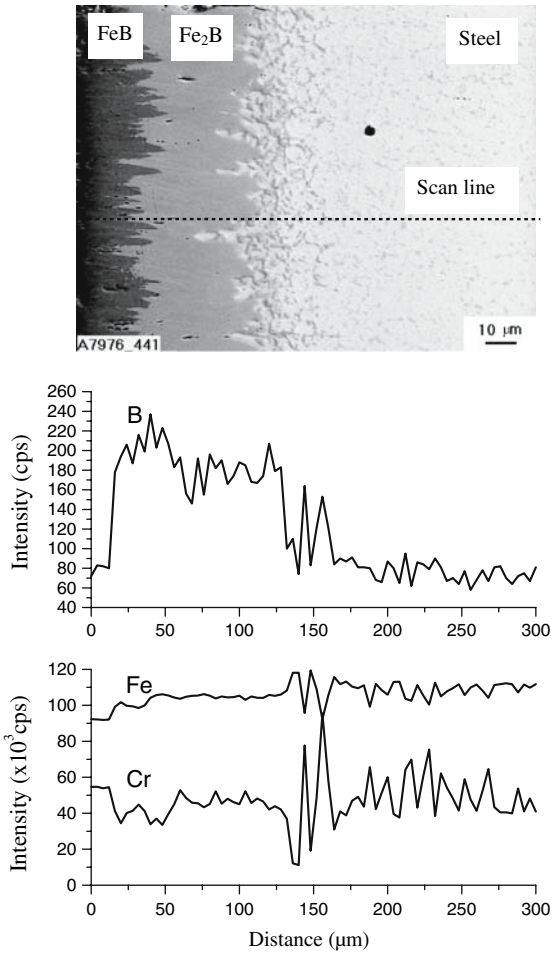

Fig. 9 Microstructure of the transition zone between a commercial 13%Cr steel and boron and concentration profiles of Fe, Cr and B. Boriding conditions: temperature 950 °C, reaction time 21600 s (6 h)

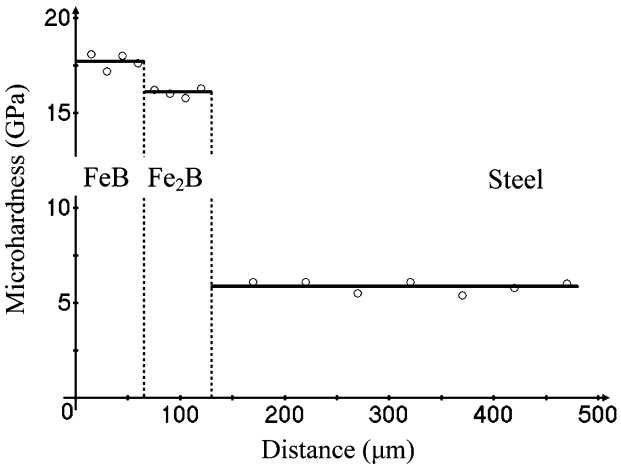

Fig. 10 A plot of microhardness, HV, against distance within reacting phases. Boriding conditions: temperature 950 °C, reaction time 21600 s (6 h)

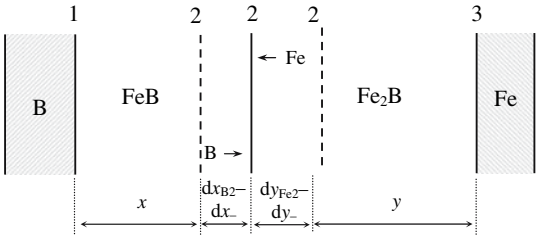

Fig. 11 Schematic diagram to illustrate the growth process of two boride layers under conditions of diffusion control. Both layers thicken at their common interface 2. No reactions take place at interfaces 1 and 3 in view of the lack of appropriate diffusing atoms

taking place at the FeB–Fe_2B and the Fe_2B-steel interfaces, respectively.

It should be noted that the growing and non-growing FeB layers behave quite differently. Unlike the diffusionally growing FeB layer, not sharing boron atoms with its neighbor Fe_2B, the non-growing one not only shares those atoms with Fe_2B but also forms an additional molecule of Fe_2B as a result of its own decomposition (for more examples of such a behavior of compound layers, see Ref. [10]).

As seen in Fig. 14b, c, the FeB layer, initially compact and around 50 μ m thick, disintegrates during vacuum annealing into separate grains and after a 12 h hold at 950 °C disappears almost completely. Grain-boundary diffusion appears to play a significant, if not decisive, role in this process because usually compound layers are consumed as a whole at their interfaces with adjacent layers, with their compactness retaining and their thickness decreasing.

Abrasive wear resistance of boride layers

Boriding the steel tablets for abrasive wear resistance tests was performed at 950 °C for 6 h, producing the (Fe,Cr)B and $(Fe,Cr)_2B$ layers of close thickness (about 110 μ m in total). Six consecutive tests were carried out on each

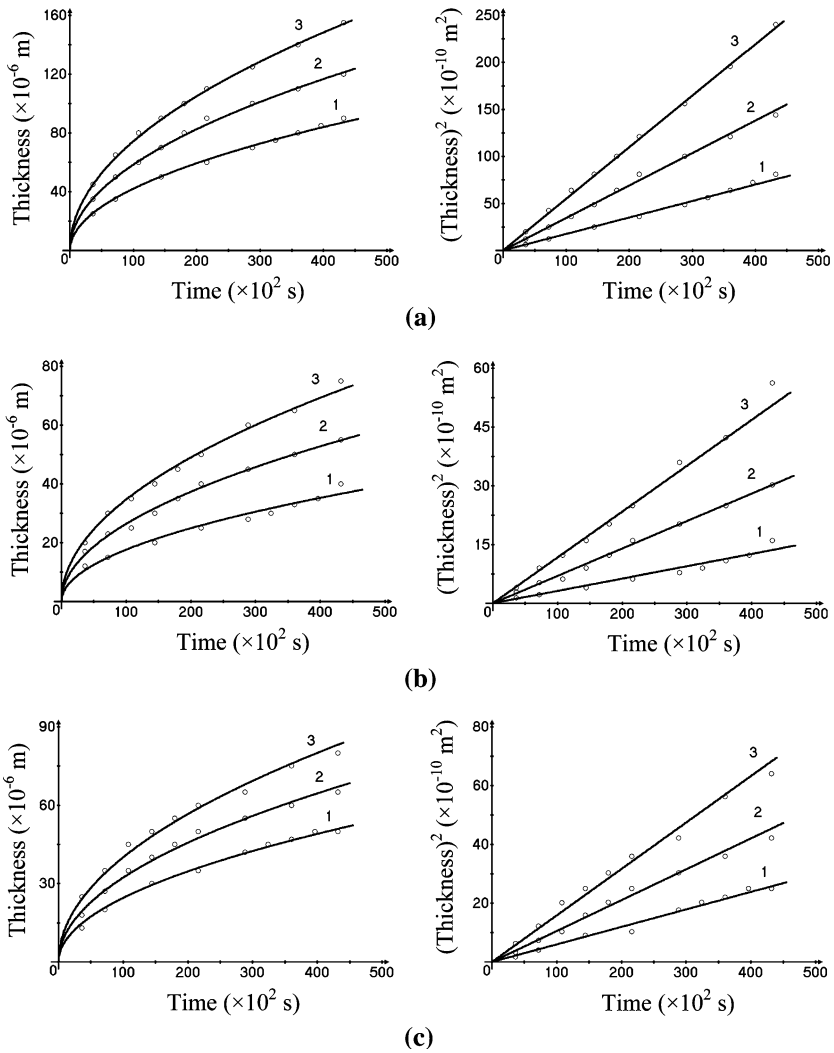

Fig. 12 Plots of layer thickness (left) and squared layer thickness (right) against time for (**a**) both boride layers, (**b**) the FeB layer and (**c**) the Fe_2B layer at a temperature of 850 °C (line 1), 900 °C (line 2) and 950 °C (line 3)

Table 6 Thickness and growth constants of the FeB and Fe_2B layers formed at the steel-boron interface

Temperature (°C)	Time ($\times 10^2$ s)	x ($\times 10^{-6}$m)			k_1 ($\times 10^{-14}$ m^2 s^{-1})			k ($\times 10^{-13}$ m^2 s^{-1})*	
		Total	FeB	Fe_2B	Total	FeB	Fe_2B	k_B	k_{Fe}
850	36	25	12	13	8.7	2.0	2.3		
	72	35	15	20	8.5	1.6	2.8	1.54	3.13
	144	50	20	30	8.7	1.4	3.1	0.94	2.01
	216	60	25	35	8.3	1.5	2.8	0.94	1.88
	288	70	28	42	8.5	1.4	3.1	1.03	2.23
	324	75	30	45	8.7	1.4	3.1	1.19	2.46
	360	80	33	47	8.9	1.5	3.1	1.31	2.56
	396	85	35	50	9.1	1.5	3.2	1.53	2.83
	432	90	40	50	9.4	1.9	2.9		
900	36	35	17	18	17.0	4.0	4.5		
	72	50	23	27	17.4	3.7	5.1	2.08	3.56
	108	60	25	35	16.7	2.9	5.7	1.84	3.72
	144	70	30	40	17.0	3.1	5.6	2.38	4.37
	180	80	35	45	17.8	3.4	5.6	2.78	4.91
	216	90	40	50	18.8	3.7	5.8	3.17	5.46
	252	100	45	55	17.4	3.5	5.3	3.57	6.00
	288	110	50	60	16.8	3.5	5.0	2.98	4.91
	360	120	55	65	16.7	3.5	4.9		
950	36	45	20	25	28.1	5.6	8.7		
	72	65	30	35	29.3	6.3	8.5	4.02	6.60
	108	80	35	45	29.6	5.7	9.3	3.30	6.03
	144	90	40	50	28.1	5.6	8.7	3.17	5.46
	180	100	45	55	27.8	5.6	8.4	3.57	6.00
	216	110	50	60	28.0	5.8	8.3	3.60	5.80
	288	125	60	65	27.1	6.3	7.3	3.57	5.32
	360	140	65	75	27.2	5.9	7.8	1.77	2.98
	432	155	75	80	27.8	6.5	7.4		

* Mean values: $k_B = (1.21 \pm 0.36) \times 10^{-13}$ m^2 s^{-1} and $k_{Fe} = (2.44 \pm 0.62) \times 10^{-13}$ m^2 s^{-1} at 850 °C, $k_B = (2.68 \pm 0.69) \times 10^{-13}$ m^2 s^{-1} and $k_{Fe} = (4.70 \pm 0.86) \times 10^{-13}$ m^2 s^{-1} at 900 °C and $k_B = (3.29 \pm 0.83) \times 10^{-13}$ m^2 s^{-1} and $k_{Fe} = (5.45 \pm 0.97) \times 10^{-13}$ m^2 s^{-1} at 950 °C

Table 7 Values of layer growth-rate constants found from a parabolic relation, k_1, and from Eqs. (2), k

Temperature (°C)	k_1 ($\times 10^{-14}$ m^2 s^{-1})			k ($\times 10^{-13}$ m^2 s^{-1}) from experimental points		k ($\times 10^{-13}$ m^2 s^{-1}) from approximated dependences	
	total	FeB	Fe_2B	k_B	k_{Fe}	k_B	k_{Fe}
850	8.8	1.6	3.0	1.21	2.44	1.04	2.01
900	17.3	3.5	5.3	2.68	4.70	2.17	3.74
950	28.1	5.9	8.3	3.29	5.45	3.61	5.96

borided steel sample, with each test along a fresh track (27.0 m long) on emery paper. The results obtained are presented in Table 8, where the data for a non-borided steel sample (one test, 27.0 m) are also given for comparison.

The wear resistance of the (Fe,Cr)B layer, found from mass loss measurements, is about 25 times greater than that of the alloy base. Deeper portions of (Fe,Cr)B coatings display a higher wear resistance compared to near-surface ones due to a more profound texture and a much less amount of cracks. The wear resistance of the inner $(Fe,Cr)_2B$ layer is around 15 times greater than that of the steel base.

Comparing the wear resistance of the outer boride coating on the surface of the steel and Fe–Cr alloys containing 10 and 25% Cr [22], it may be concluded that its value for the steel and an Fe–10% Cr alloy are rather close,

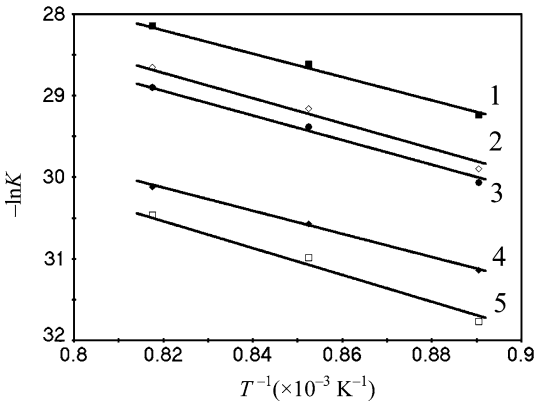

Fig. 13 The temperature dependence of the layer growth-rate constants, K: 1, k_{Fe}; 2, k_B; 3, k_1 for both boride layers; 4, k_1 for Fe_2B; 5, k_1 for FeB

with the coating on the steel surface being about 15% more resistant than that on the alloy surface. The FeB coating on both materials is much less resistant (by an order of magnitude) than that on an Fe–25% Cr alloy. Most probably, it is due to structural or morphological rather than compositional reasons.

Conclusions

Two boride phases FeB and Fe_2B occur as separate layers at the interface between a commercial 13%Cr steel (40X13) and a mixture of amorphous boron with 5% KBF_4 at 850–950 °C and reaction times up to 12 h. The average content of chromium is around 8 at.% in the outer FeB layer and 9 at.% in the inner Fe_2B layer.

The characteristic feature of both layers is a pronounced texture. The strongest reflections are {002} and {020} for the orthorhombic FeB phase and {002} for the tetragonal Fe_2B phase.

Diffusional growth kinetics of the boride layers are close to parabolic. Alternatively, layer-growth kinetics can be described by a system of non-linear differential equations, also producing a good fit to the experimental data.

Annealing of a borided steel sample in the absence of boriding media causes the disappearance of the FeB layer. Grain-boundary diffusion appears to play a significant role in this process.

Microhardness values are 17.9 ± 1.5 GPa for the FeB layer, 16.1 ± 0.9 for the Fe_2B layer and 5.9 ± 0.3 GPa for the steel base. Microhardness is practically constant within both boride layers.

The abrasive wear resistance of the FeB layer, found from mass loss measurements, is approximately 25 times greater than that of the steel base. The Fe_2B layer yields about a 15-fold increase in wear resistance of steel samples.

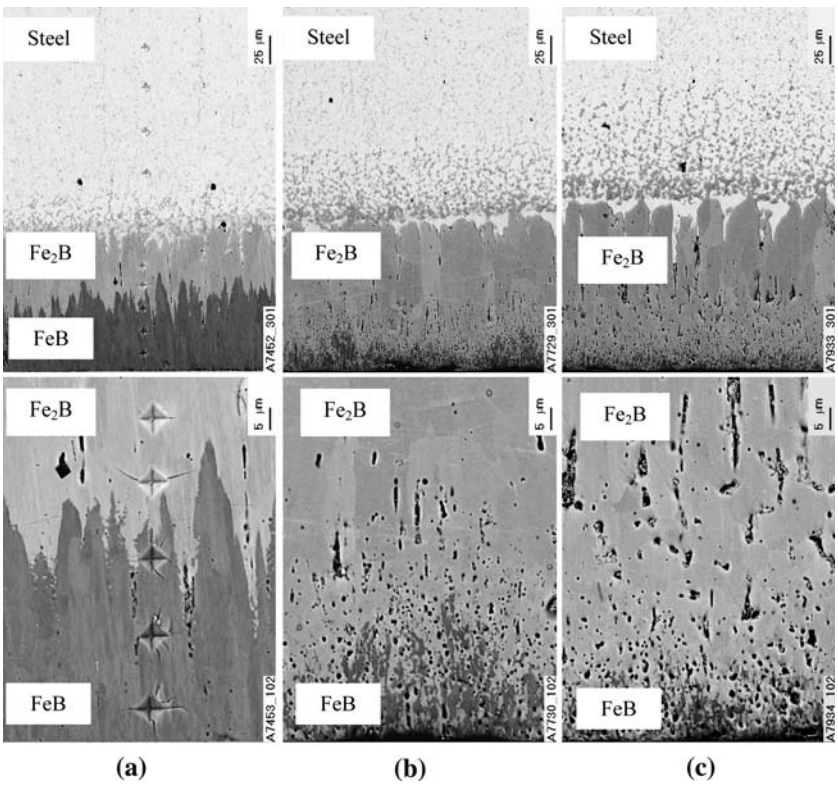

Fig. 14 Backscattered electron images at different magnification illustrating the process of degradation of boride layers during vacuum annealing at a temperature of 950 °C in the absence of the boriding mixture: (**a**) as-received condition, (**b**) 6 h annealing and (**c**) 12 h annealing

Table 8 Results of abrasive wear resistance tests of borided steel samples. Boriding conditions: temperature 950 °C, reaction time 21600 s (6 h). Six consecutive tests (each along a fresh track, 27.0 m long) were carried out on each of three borided samples. Mean values for each test are presented (deviation ±15%). For comparison, one test (27.0 m) was performed on a non-borided steel sample

Serial test number	Δm (g)*	$\Delta m_{steel} : \Delta m_{boride}$	Δh (mm)	Phase
1	0.02817	11.8	0.025	(Fe,Cr)B
2	0.01290	25.8	0.015	(Fe,Cr)B
3	0.01857	17.9	0.020	(Fe,Cr)B + $(Fe,Cr)_2B$
4	0.02117	15.7	0.025	$(Fe,Cr)_2B$
5	0.03977	10.0	0.035	$(Fe,Cr)_2B$ + steel base
6	0.05400	6.6	0.045	$(Fe,Cr)_2B$ + steel base
1	0.3329	–	0.40	Non-borided sample

* Δm and Δh are changes in mass and height, respectively, of samples.

Acknowledgements This investigation was supported in part by the STCU grant No. 2028. The author is grateful to V. G. Khoruzha, V. R. Sidorko, K. A. Meleshevich and A. V. Samelyuk for their help in conducting the experiments and carrying out the necessary analyses.

References

1. Voroshnin LG, Lyakhovich LS (1978) Borirovaniye stali. Metallurgiya, Moskwa, (in Russian)
2. Kunst H, Schroll H, Luetje R, Wittel K, Lugscheider E, Weber T, Eschnauer HR, Raub C (1991) In: Ullmann's Encyclopedia of Industrial Chemistry, vol A16. Verlag Chemie, Weinheim, p 427
3. Sinha AK (1982) Boriding (Boronizing). In: Sinha AK (ed) Metals Handbook. ASM International, Metals Park OH, p 844
4. Hansen M, Anderko K (1958) Constitution of binary alloys, 2nd edn. McGraw-Hill, New-York, p 249
5. Vol AE (1962) Stroeniye i svoystva dvoynikh metallicheskikh system, vol 1. Fizmatgiz, Moskwa, p 679 (in Russian)
6. Massalski TB, Murray JL, Bennett LH, Baker H (eds) (1986) Binary Alloy Phase Diagrams, vol 1. American Society of Metals, Metals Park OH, p 351
7. Okamoto H (2004) J Phase Equilib Diffusion 25:297–298
8. Brandstötter J, Lengauer W (1997) J Alloys Compd 262–263:390–396
9. Gurov KP, Kartashkin BA, Ugaste YuE (1981) Vzaimnaya diffusiya v mnogofaznikh metallicheskikh sistemakh. Nauka, Moskwa, (in Russian)
10. Dybkov VI (2002) Reaction diffusion and solid state chemical kinetics. The IPMS Publications, Kyiv, (free access at http://users.i.com.ua/~dybkov/V)
11. Voroshnin LG (1981) Borirovaniye promyshlennikh staley i chugunov. Belarus, Minsk, (in Russian)
12. Dybkov VI, Lengauer W, Barmak K (2005) J Alloys Compd 398:113–122
13. Gorelik SS, Rastorguev LN, Skakov YuA (1970) Rentgenograficheskiy i elektronno-opticheskiy analiz, prilozheniya. Metallurgiya, Moskwa, p 29 (in Russian)
14. Carbucicchio M, Palombarini G (1987) J Mater Sci Lett 6: 1147–1149
15. Martini C, Palombarini G, Carbucicchio M (2004) J Mater Sci 39:933–937
16. Seith W (1955) Diffusion in metallen. Springer, Berlin
17. Hauffe K (1955) Reaktionen in und an festen Stoffen. Springer, Berlin
18. Arkharov VI (1959) Fiz Metall Metalloved 8:193–204
19. Schröder B, Leute V (1980) J Phys Chem Solids 41:827–835
20. . Fromhold AT, Sato N (1981) Oxid Metals 16:203–220
21. Dybkov OV, Dybkov VI (2004) J Mater Sci Lett 39:6615–6617
22. Dybkov VI, Lengauer W, Barmak K (2005) In: Proc 16th Plansee Seminar, Reutte, Austria, May 31-June 4, 2:999–1009